Conformational Analysis of Ketolide, Conformations of RU 004 in Solution and Bound to Bacterial Ribosomes

Gildas Bertho,[†] Josyane Gharbi-Benarous,[†,‡] Marcel Delaforge,[†] Catherine Lang,[§] Annick Parent,[§] and Jean-Pierre Girault*[,†]

Université René Descartes-Paris V, Laboratoire de Chimie et Biochimie Pharmacologiques et Toxicologiques (URA 400 CNRS), 45 rue des Saint-Pères, 75270 Paris Cedex 06, France, Université Denis Diderot-Paris VII, UFR Chimie, 2 Place Jussieu, F-75251 Paris Cedex 05, France, and Hoechst Marion Roussel, 102 route de Noisy, 93235 Romainville Cedex, France

Received December 19, 1997

A new structurally distinct class of 14-membered-ring macrolides is characterized by a keto-function instead of the cladinose sugar, well-known for its fragility even in weakly acidic media. This new class called ketolides is endowed with remarkable antibacterial activity against macrolide-resistant strains. A complete assignment of the ^{1}H and ^{13}C NMR spectra of RU 004 in deuteriochloroform, methanol-d_4 and D_2O has been made using different two-dimensional (2D) chemical-shift correlation methods. The study of ketolide−ribosome interaction has been investigated using 2D transferred nuclear Overhauser effect spectroscopy (TRNOESY). A comparison of the conformations in solution and bound to ribosomes was made with those of previous macrolides. This study can highlight some of the significant differences between RU 004 and other antibiotics.

Introduction

Macrolides are an old well-known family of oral antibiotics.[1] Resistance to macrolides has increased in several areas around the world due to extensive therapeutic use. A new distinct class of semisynthetic antibiotic called ketolides is endowed with remarkable antibacterial activity against macrolide-resistant strains.[2−4] In this new class of ribosome-targeted antibiotics, the cladinose moiety is replaced by a keto function, whereas this sugar was long thought to be essential for antibacterial activity. RU 004 is synthesized from the 3-keto 6-methoxy erythromycin skeleton and has a quinoline side chain linked to the 11-12 position by an original cyclic hydrazono-carbamate function. The original chemical structure and the outstanding antibacterial activity of ketolides[2−8] qualify them to be part of a separate class of the 14-membered-ring macrolide family.

Acid stability experiments of ketolides versus macrolides demonstrate the high stability of ketolides precluding any chemical degradation. The cladinose sugar is an acid labile group which can be hydrolyzed in gastric media leading, in the case of the parent macrolide erythromycin A, to the intramolecular cyclization which destroys its antibacterial activity.[9]

Some 14-membered-ring macrolides cause clinical drug interactions, resulting in altered metabolism of concomitantly administered drugs via formation of an inactive and stable cytochrome P-450 complex.[10,11] Unlike macrolides, ketolides do not form any detectable metabolic intermediate complex (nitroso complexes were detected neither in vitro nor in vivo, after repeated doses of RU 004), whatever the type of interaction or the affinity constants for the P-450, 3A isozyme family. Thus, little or no drug−drug interaction is expected with ketolides.[3,12]

RU 004 may be a good candidate for further investigation in the development of new antiinfectives and its physicochemical properties remain to be fully characterized.

RU 004

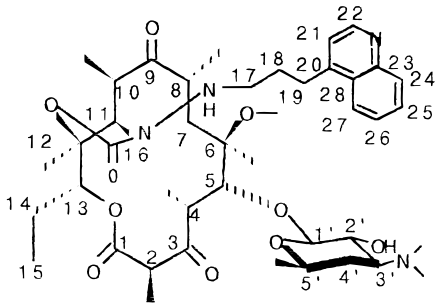

pKa1 = 5,3 pKa2 = 8,6

Erythromycin, roxithromycin, and their derivatives exert their antibacterial action by binding to bacterial ribosomes, specifically to the 50S subunit. There appear to be two stages to this binding, a weak interaction which can be detected by NMR spectroscopy,[13,14] and a stronger interaction ($K_d = 10^{-7}$ to 10^{-9} M)[15−17] detected by equilibrium dialysis and related methods. The weak binding of erythromycin A to ribosomes has been characterized extensively by line broadening and transferred NOESY (TRNOESY) experiments,[13,18−20] the interaction being a fast exchange process on the NMR time scale. Two sites of interaction of ketolides on the ribosome were suggested by using kinetics and competition methodology.[21,22] It was noticed that ketolides generally showed a slightly lower affinity for the 70S

* Author to whom correspondence may be addressed. E-mail: Jean-Pierre.Girault@biomedicale.univ-paris5.fr.
[†] Université René Descartes.
[‡] Université Denis Diderot.
[§] Hoechst Marion Roussel.

S0022-2623(97)00852-2 CCC: $15.00
Published on Web 08/01/1998

ribosome target than did roxithromycin but displayed a significantly better overall antibiotic activity. To compare the behavior of RU 004, it is first necessary to assign the ^1H and ^{13}C NMR spectra of the drug. Assignments of the spectra in $CDCl_3$ and in D_2O buffer−DMSO-d_6 are reported here.

The primary goal of this work was to determine a global solution conformation of RU 004. This has been accomplished by obtaining information about dihedral angles from the vicinal coupling constant data, by acquiring the spatial proximity information from nuclear Overhauser effect data and through the use of molecular modeling by mechanics and dynamics calculations. Thus, for our studies it was necessary to make a complete unambiguous assignment of the ^1H and ^{13}C NMR spectra prior to performing conformational analysis.

Results and Discussion

Part 1. NMR. Analysis of the ^1H and ^{13}C NMR Spectra. RU 004 is much more soluble in $CDCl_3$ or CD_3OD than in buffered D_2O solution. The assignments have been made using one-dimensional (1D) ^1H and ^{13}C (^1H decoupled and DEPT-135)[23] spectra, two-dimensional (2D) homonuclear double quantum (COSY) spectra, heteronuclear multiple bond correlation (HMBC) spectra[24] and heteronuclear multiple quantum correlation (HMQC) spectra.[25−27] ^{13}C assignments were then derived from $^1H-^{13}C$ correlations including long-range INEPT experiments.[28] The ^1H and ^{13}C NMR chemical-shift and coupling-constant values for RU 004 in buffered D_2O and D_2O/DMSO (20:80) solution are listed in Table 1 and in Table S1 of the Supporting Information for RU 004 in $CDCl_3$ and CD_3OD. DMSO was used for these experiments because it showed increased solubility of RU 004 when compared with buffered D_2O solvent.

The 500 MHz ^1H NMR spectrum of RU 004 in $CDCl_3$ solution at 25 °C, is shown in Figure 1. The remaining ambiguities after the simple ^1H COSY spectrum were resolved by HMQC and HMBC experiments (Figure S1 of the Supporting Information). The connection between spin systems was given essentially via HMBC $^1H-^{13}C$ ^3J correlations. The H(11)−C(16) and H(11)−C(13) (or C(11)−H(13)) HMBC and HMQC correlations allowed us to link the spin group C(11) to the hydrazonocarbamate cycle and to the spin group C(13).

The DQF-COSY and $^1H-^{13}C$ correlation spectra were used to assign the whole of the corresponding spin group C(16) to C(28) for the quinoline chain. The strong NOE [17-NH]10-Me is the only possibility linking the macrocycle to the chain for a complete unambiguous assignment.

Buffered D_2O. RU 004 is poorly soluble in aqueous buffers (0.5 mM). RU 004 is much more hydrophobic than the parent drugs (roxithromycin or erythromycin A). Since it was not possible to obtain useful $^1H-^{13}C$ correlation spectra in D_2O solution, D_2O buffer−DMSO-d_6 (20:80) solutions (4 mM) were used.

Initially, the solution of RU 004 at pH 7.6 was used to obtain ^1H, DQ-COSY, and ^1H NOESY spectra at 500 MHz. Proton assignments at physiological pH could be deduced from the ^1H spectrum of RU 004 in $CDCl_3$. In buffered D_2O, there was no sign of a second compound being formed, which is different from the situation with erythromycin A. In aqueous or D_2O−DMSO-d_6 (20:80) solutions, RU 004 exists as a single compound (as discerned by NMR), whereas erythromycin contains up to 40% of the 12,9-hemiketal at 293 K. The presence of the *O*-methyl group on C(6) and 11,12-cyclic hydrazonocarbamate function prevent both 6,9- and 12,9-cyclization. RU 004 differs also from erythromycin by the 3-keto function in place of the cladinose moiety. This modification has substantial effects on the C(3)−C(6) region of the erythromycin skeleton.

The TOCSY spectrum was used to distinguish the major spin groups, and the COSY spectrum was used to confirm the assignments of the hydrogen resonances within each spin group. The singlet at δ 2.85 corresponding to 3′−$N(CH_3)_2$ was assigned by inspection. The chemical shifts of the *N*,*N*-dimethyl protons will depend

Table 1. ^1H and ^{13}C NMR Spectra of RU 004 in D_2O−DMSO (20:80, 4 mM) and D_2O (0.5 mM, pH 7.6) Buffered Solutions

site	δ_H	δ_H[a]	δ_C[a]	$J_{^1H^1H}$[b]
1			169.6	
2	*c*	*c*	49.8	
2-Me	1.30	1.25	15.3	
3			204.4	
4	3.17	3.12	46.9	6.9; 8.2(8.4)
4-Me	1.21	1.25	14.1	6.9
5	4.13	4.12	78.5	8.2(8.4)
6			77.7	
6-Me	1.08	1.23	20.0	
6-OMe	1.80	2.47	49.8	
7-a	1.68	1.64	38.4	
7-b	1.79	1.74		
8	2.55	2.56	43.3	6.0(6.4)
8-Me	1.20	1.18	17.7	6.0(6.4)
9			218.1	
10	3.35	3.27	39.4	6.8(6.6; 1.5)
10-Me	1.01	0.98	13.6	6.8(6.6)
11	3.48	3.71	58.1	(1.5)
12			80.7	
12-Me	1.56	1.55	14.1	
13	4.68	4.83	76.6	9.9(9.7); 2.4
14-a	1.62	1.64	21.9	9.9(9.7); 7.4(7.3)
14-b	1.76	1.74		2.4; 7.4(7.3)
15-Me	0.74	0.76	10.5	7.4(7.3)
16			155.4	
17-NH		5.41		
17A	2.76	2.80	47.5	
17B	2.70			
18A	2.07	1.84	28.5	
18B	2.01			
19A	3.36	3.29	28.9	
19B	3.25	3.15		
20				
21	7.46	7.45	121.4	4.5(4.3)
22	8.73	8.80	150.3	4.5(4.3)
23			147.6	
24	8.07	8.08	129.2	8.6(8.6)
25	7.84	7.83	129.6	8.6(8.6)
26	7.70	7.66	126.7	8.3(8.4)
27	8.25	8.24	124.0	8.3(8.4)
28			126.6	
1′	4.44	4.21	103.7	6.4(7.4)
2′	3.49	3.13	70.2	6.4(7.4)
3′	3.49	2.60	64.1	
3′-N(Me)2	2.85	2.26	40.3	
4′-ax	1.58	1.18	30.7	−12.5; 10.7
4′-eq	2.17	1.71		−12.5
5′	3.84	3.56	68.6	10.7; 6.1
5′-Me	1.39	1.21	20.9	6.1

[a] Chemical shifts are determined in D_2O (buffered pH,7.6)−DMSO (20:80) solution. [b] Coupling constants determined in D_2O (buffered pH,7.6)−DMSO (20:80) solution are given in parentheses. [c] Protons are exchanged with solution (probably by tautomery).

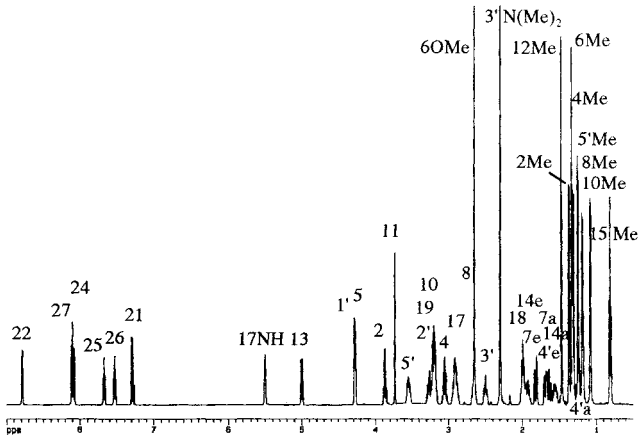

Figure 1. 500 MHz proton spectrum of a 38 mM solution of RU 004 in $CDCl_3$. Selected signals are identified.

on the state of ionization of that group.[29] One observes, in D_2O solution, that the amino group signal of RU 004 at 2.85 ppm, is similar to the resonance of the methyl in the protonated form.

^{13}C, DEPT135, $^1H-^{13}C$ correlation spectra (HMQC and HMBC) were obtained using the D_2O buffer−DMSO-d_6 (20:80) solution (4 mM). HMQC and HMBC spectra completed the assignments of the quinoline chain in D_2O buffer−DMSO-d_6 (20:80) solution, and no significant changes in chemical shifts were observed throughout the chain. The DEPT 135 and $^1H-^{13}C$ correlation spectra were then used to assign the ^{13}C signals corresponding to the ^1H spin groups already assigned. The quaternary ^{13}C signals, the isolated *C*-methyl groups, the *O*-methyl-6, and the C(2) carbon remained to be assigned. However, no cross-peak could be located for C(2), and no signal was seen in the ^{13}C spectrum which might be assignable to C(2). In the same way, CH_3-2 appears as a singlet (doublet in $CDCl_3$) because the H(2) was exchanged in D_2O, presumably in the tautomeric equilibrium of the β-keto-ester enolate form. In the HMBC spectrum, C(2) was assigned from CH_3-2.

C(6) showed cross-peaks, surprisingly, to the methyl groups δ_H 1.08 and 1.80 in D_2O and 1.23 and 2.47 in D_2O buffer−DMSO-d_6 (20:80). These signals were assigned to CH_3-6 and OCH_3-6, respectively, and the corresponding ^{13}C assignments were deduced from the $^1H-^{13}C$ spectrum. The upfield shifts seen for CH_3-6 and OCH_3-6 (^1H spectrum) resonances are caused by the shielding effect of the steric interactions with the aromatic nucleus. A comparison of the chemical shifts of 6-OMe-roxithromycin (9-oxime chain and 6-*O*-methyl) or clarithromycin (9-ketone and 6-*O*-methyl) and RU 004 is interesting. In the ^{13}C and ^1H spectra in $CDCl_3$, for example, H(5), CH_3-6, and OCH_3-6 show differences of more than 1 ppm. In D_2O buffer, the situation is amplified in the 1−2 ppm range (in this case the OCH_3-6 has been shifted by about 2 ppm because of differences in quinoline chain position; this shift has been taken into account in molecular modeling).

Conformational Analysis. The notations for macrocycle, desosamine, ethyl, and quinoline chain conformer designations are defined as **M**, **D**, **T**, and **C**, respectively, in Table S2 of the Supporting Information together with some of their characteristics.

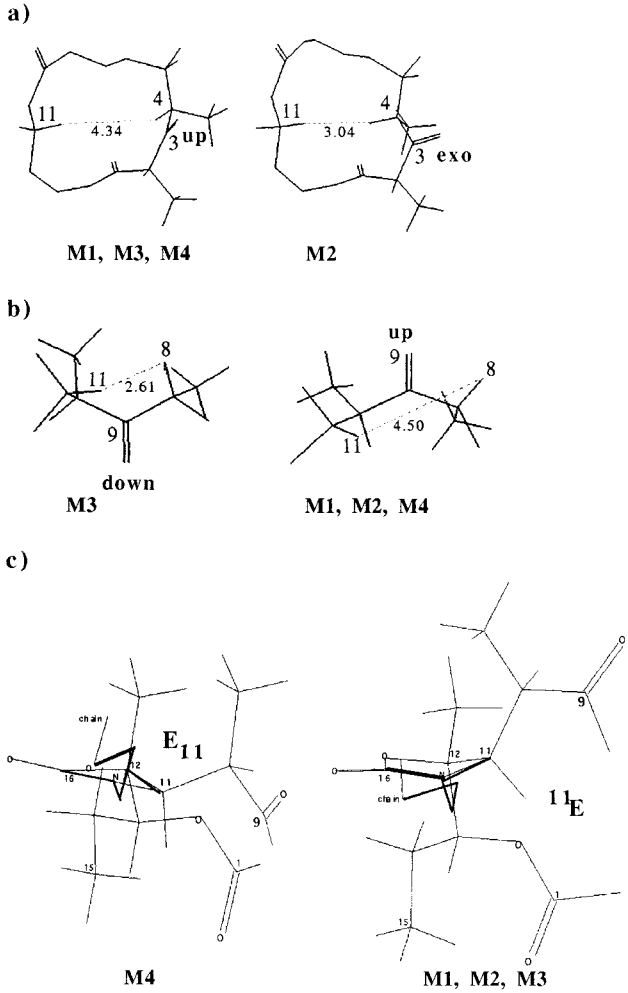

Figure 2. (a) An "exo" orientation of CO-3 group in **M2**. (b) The fluctuation of the 9-CO group above or below the plane of the erythronolide leads to the conformation **M3**. (c) Conformation **M4** differs in the inward folding of the envelope E_{11} representing the five hydrazono-carbamate cycle. The envelope forms interconvert by the pseudorotation process of the 5-membered ring, and two flexible forms exist, namely, envelope E_{11} (**M4**) and ^{11}E (**M1**−**M3**) conformers.

The conformations of the lactone ring (Figure 2) were termed **M1**−**M4**. The major conformer **M1** was characterized by the "up" position of the three carbonyl groups (1-CO, 3-CO, and 9-CO) while an "exo" orientation of the 3-CO group leads to the conformation **M2**. Conformation **M3** is observed when the fluctuation of the 9-CO group leads to a "down" orientation with respect to the macrocycle. The inward folding of the envelope E_{11} representing the five hydrazono-carbamate cycle is the major change observed in conformation **M4**.

The 11−12 fragment was fixed by the cyclic hydrazono-carbamate function, but the side chain C(17)−C(20) explores a large conformational space corresponding to six states (**C1**−**C6**) (Figure 3a). Contacts of the quinoline chain with the erythronolide are nonexistent in **C5**, and thus there is a total release of this unit that is no longer maintained by stacking. When the quinoline chain overlaps the macrolactone ring, the chain is tightly bound to the erythronolide, giving typical stacking conformations such as **C1**−**C4** and **C6**. The position of the aromatic nucleus may allow the π electron of the nitrogen of the quinoline to interact in terms of attrac-

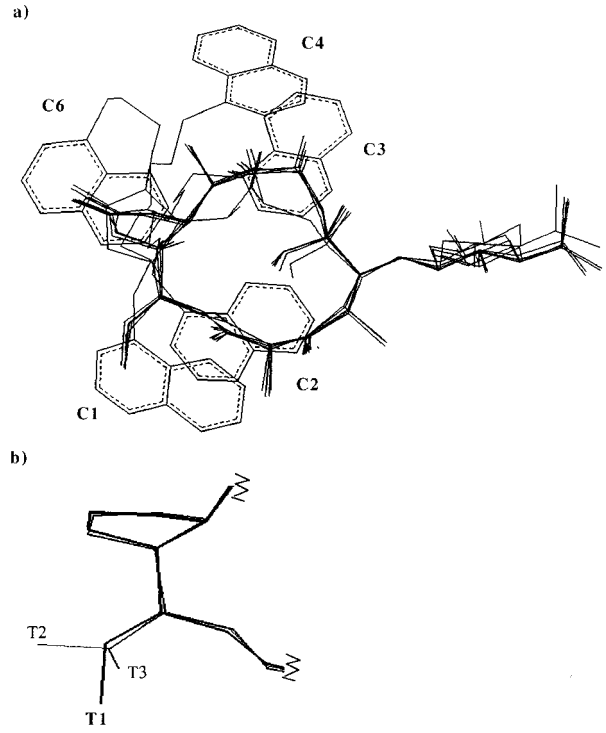

Figure 3. (a) The five stacking conformers of the quinoline with the aromatic nucleus above the ethyl group (**C1**) or the carbonyl groups: 1-CO (**C2**), 9-CO (**C4**), 16-CO (**C6**) or the 6-OMe group (**C3**). (b) The ethyl group leads to three **T1**−**T3** positions: parallel (*t*) **T1** and perpendicular (g^-) **T2** and (g^+) **T3** to the macrocycle.

tive potential with carbonyl groups, 1-CO (**C1**), 3-CO (**C2**), 9-CO (**C4**), and 16-CO (**C6**) ($\pi-\pi$ interactions) and with the methoxy group, 6-O (**C3**) of the macrocycle.

Moreover, the fluctuation of the C(13)−C(14) moiety of the lactone ring gives rise to a free rotation of the ethyl group which can take up three positions (**T1**−**T3**), parallel (*t*) **T1** and perpendicular (g^-) **T2** or (g^+) **T3** to the macrocycle (Figure 3b).

The macrocycle flexibility induces four different orientations **D1**−**D4** for the desosamine sugar (Figure 4). The nonsimilarity in ϕ_{C4C5} of the two structures **M1** (−70°) and **M2** (−115°), respectively, implies that the orientation of the sugar ring with respect to the macrocycle is not the same for both conformations (**D1** and **D2**). In the **M2** conformation of the macrocycle, rotation about the C3−C4−C5 bonds leads to a decrease of ca. 50° in ϕ_{C4C5} with respect to the **M1D1** structure. The proton H(4) folds inside the erythronolide, and then the desosamine sugar moves down. However, its orientation perpendicular to the macrocycle remains unchanged. This modification does not affect in a significant manner the sugar position (noted **D2**), but shifting of the desosamine dimethyl amino group with modifications of the bond angle and steric hindrance in the 3-keto-4-methyl area may be of importance for the ketolide mode of action. Conformers **D1** and **D2** exhibit an orientation of the desosamine nearly perpendicular to the macrocycle, whereas the two units (desosamine and macrocycle) are in the same plane in conformations **D3** and **D4**. In the **D4** position, the desosamine sugar is coplanar to the macrocycle with a "turn back" of 180° relative to the orientation **D3**.

A combination of NMR studies and molecular modeling has been used to predict the major conformation of

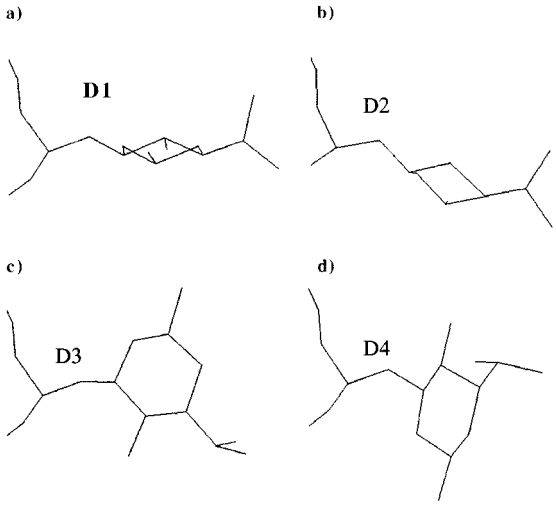

Figure 4. Conformations of the desosamine sugar ring following its orientation with respect to the lactone ring and the glycosidic dihedral angles, ψ_1, H(5)−C(5)−O(5)−C(1′), ψ_2, C(5)−O(5)−C(1′)−H(1′): two orientations are perpendicular to the macrocycle **D1** (ψ_1, 10°, ψ_2, 55°) and **D2** (ψ_1, 25°, ψ_2, 50°) which are induced by the **M2** conformer; in the **D4** (ψ_1, 15°, ψ_2, 140°) position, the desosamine sugar is coplanar to the macrocycle with a turn back of 180° relative to the orientation **D3** (ψ_1, −20°, ψ_2, −10°).

RU 004 in solution and its similarity to the crystalline conformations. The identities and proportions of the different isomers in aqueous solution were of special interest. An analysis of the ^{1}H NMR coupling constants [$^3J_{H,H}$ values] was also used to predict the similarity, specifically the environment around the C(13)−C(1)−C(7) region, between the major solution conformation of RU 004 and those of 14-membered-ring macrolides. For example, the bound conformations of 6-OMe-roxithromycin and clarithromycin show conformational homology in this region when the two macrolides exert their antibacterial action by binding to bacterial ribosomes.[30]

Two crystal structures of RU 004 were identified,[22] and they present different characteristics as shown by X-ray analysis (Figure 5a) {(i) Crystal data S^- obtained in methylene chloride and cyclohexane (1 molecule of solvent, cyclohexane is stacked between the quinoline chain and the macrocycle): orthorhombic crystal; a = 36.3 Å, b = 12.16 Å, c = 11.3 Å; space group $P2_12_12_1$; R = 9.9 and (ii) crystal data $\mathbf{S}^+$ obtained in acetone: tetragonal crystal; a = 11.66 Å, b = 11.66 Å, c = 63.9 Å; space group $P4_12_12_1$; R = 4.7. The structures are referred to $\mathbf{S}^+$ or $\mathbf{S}^-$ because the last rotor corresponding to the alkyl part of the chain, the C(19)−C(20) dihedral angle is either g^- ($\mathbf{S}^-$) or g^+ ($\mathbf{S}^+$) (Figure 5b)}. The structures of RU 004 obtained by X-ray diffraction (Figure 5) revealed an interesting feature of the erythronolide ring (**M1T1**) with the 11,12-quinoline chain directed up above it (**C5**). In the solid state, the desosamine sugar (**D1**) is oriented perpendicular to the macrocyclic lactone ring.

Homonuclear $^3J_{^1H-^1H}$ and Heteronuclear $^3J_{^{13}C-^1H}$ Coupling Constants. Initially, it was felt that much of the conformational information could be deduced from the ^{1}H−^{1}H coupling constant data given in Table 1 (and in Table S1). Our observed values were compared to those of the minimized structures generated by molec-

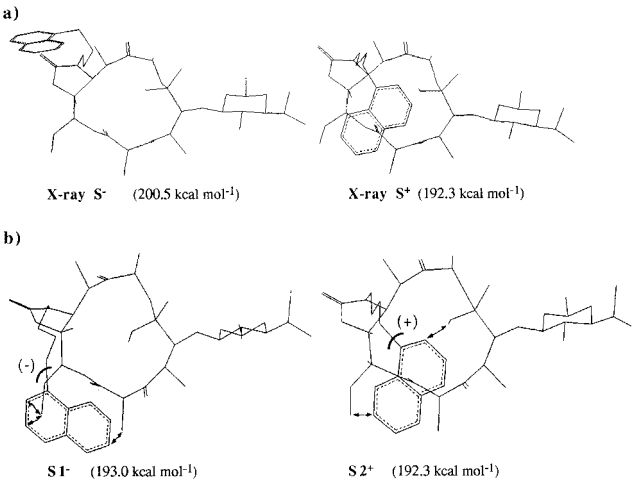

Figure 5. (a) Two crystal structures of RU 004 were identified, crystal data $\mathbf{S}^+$ and crystal data $\mathbf{S}^-$. The structures are referred to as $\mathbf{S}^+$ or S^- because the last rotor corresponding to the alkyl part of the chain, the C(18)−C(21) torsion angle, is either g^- ($\mathbf{S}^-$) or g^+ ($\mathbf{S}^+$). (b) In the lowest energy conformations, $\mathbf{S2}^+$ (192.3 kcal mol^{-1}) and $\mathbf{S1}^-$ (193.0 kcal mol^{-1}), the observed [21]6-OMe and [26]15-Me NOEs are indicative of a **C2**-(+) conformation of the quinoline chain which is held between 1-CO and 3-CO ending up above 3-CO. The **C2**-(+) chain is stopped at the right-hand side by the 6-OMe group close to the contact region between the sugar units. The NOEs [21]-15-Me, [22]15-Me, and [25]2-Me are due to a **C1**-(−) position of the aromatic nucleus in the $\mathbf{S}^-$ structures. The **C1**-(−) chain seems to be pushed back toward the left part of the macrocycle, in the C(11)−C(13) region.

ular dynamics (MD) study versus the different protocols. The torsion angles of the generated structures can be correlated by using Karplus-type equations[31,32] to the corresponding coupling constants calculated in Table 2 and in Table S3 of the Supporting Information ($\mathbf{S}^-$ data).

An analysis of the $^3J_{H,H}$ values was also used to compare the major solution state conformation of RU 004 and that in the crystalline state. The observed vicinal coupling constants confirm that RU 004 exists in solution as a major conformation which is very similar to the solid state conformation ($\mathbf{S}^+$) (Table 2).

The coupling constants found in the lactone are consistent with trans-pseudo-axial (ca. 170°) and trans-pseudo-equatorial (ca. 70°) dihedral angles, except for H(4)-C(4)−C(5)-H(5), $J_{4,5} = 8.6$ Hz ($CDCl_3$) or $J_{4,5} = 8.2$ Hz (D_2O) (Tables 1−2). The difference, much larger than the experimental error (0.3 Hz), may be interpreted as a participation of a transoidal angle in an eclipsed Newman projection (**M2**) (Figure 2a).

$$\mathbf{M1}\ \text{conformation}\ J_{calc}(168°) = 10.9\ \text{Hz}$$

$$\mathbf{M2}\ \text{conformation}\ J_{calc}(118°) = 4.1\ \text{Hz}$$

So, the observed $^3J_{4,5} = 8.6$ Hz, would correspond effectively to $^2/_3J_t + {}^1/_3J_g$, where J_t and J_g are trans (**M1**) and gauche (**M2**) coupling constants, respectively.

Additionally, the extreme difference between the values of the coupling constants ($J_{7,8} = 12.3$, $J_{13,14} = 10.7$, and $J_{10,11} \approx 1$ Hz) and those of the calculated ones suggests that any fluxional motion is limited to the C(4)−C(5) torsional angle or involves multiple bonds (CO-1, CO-3, CO-9, and CO-16) and the envelope E_{11} representing the five cyclic hydrazono-carbamate function (Figure 2c).

The ethyl group is conformationally flexible (Figure 3b), and thus, the observed $^3J_{13,14} = 10.7$ Hz would correspond to 5% J_g + 95% J_t, where J_g and J_t represent the coupling constants, gauche (2.5) for the minor **T2**−**T3** forms and trans (11.0) for the major **T1** one, respectively.

An analysis of ^3J values was used to predict the conformational analysis of the three flexible units (macrocycle, quinoline chain, and particularly desosamine sugar). The determination of long-range $^3J_{^{13}C,^1H}$ coupling constants provides important structural information for macrolide antibiotics.[33]

A specific characterization of an "exo" orientation of the CO-3 group in **M2** (Figure 2a) will be given by the use of the $^3J_{H(4),H(5)}$ (mentioned above) and $^3J_{H(5),C(3)}$ coupling constants: H(5) and C(3) are either eclipsed (0°) in **M2** or gauche (55°) in **M1**, **M3**, and **M4**. The experimental coupling constant $^3J_{H(5),C(3)}$ (2.0 Hz) is in agreement with a major presence of the low-energy conformation **M1**.

The major change between **M1** and **M4** conformations is the interconversion of the envelope E_{11} (**M4**) representing the five hydrazono-carbamate cycle in the envelope ^{11}E (**M1**−**M3**), by the pseudorotation process of the 5-membered ring (Figure 2c).[34] An accurate description of the ring will be given by the use of the $^3J_{H(11),CMe(12)}$ and $^3J_{H(11),C(16)}$ coupling constants. The comparison between calculated (Table 2) and experimental values ($^3J_{H(11),CMe(12)} = 0.8$ Hz and $^3J_{H(11),C(16)} = 3.7$ Hz) allowed us to define the ^{11}E (**M1**−**M3**) conformation as the major one in solution.

The measurement of heteronuclear long-range $^3J_{^{13}C-^1H}$ coupling constants by selective 2D INEPT[33] combined with studies by MD (Table 2) was useful to identify the positions and mobility of the desosamine sugar with respect to the erythronolide (Figure 4). This is of particular interest since it can be related to the different biological properties of the macrolides. The glycosidic bond orientations Ψ_1 = H(5)−C(5)−O(5)−C(1′) and Ψ_2 = H(1′)−C(1′)−O(5)−C(5) were studied by selective excitation of the protons H(5) and H(1′), respectively. Experimental values ($J_{\Psi 1}$ and $J_{\Psi 2}$) are discussed with regard to the calculated values in the different **D1**−**D4** conformers from lowest energy structures (Table 2). The presence of the major **D1** conformation should increase the coupling constant corresponding to Ψ1 and, at the same time, decrease that of Ψ_2. However, the participation of the other conformations should decrease the value of $J_{\Psi 1}$ and increase that of $J_{\Psi 2}$. The observed values for $J_{\Psi 1}$ (6.2 Hz) and $J_{\Psi 2}$ (2 Hz) should include a large participation of conformer **D1**, and this was confirmed by NOEs experiments.

All these conclusions will be further tested using MD experiments.

Nuclear Overhauser Enhancement Experiments. Unfortunately, the environment surrounding the quinoline group could not be determined accurately by vicinal coupling constants. In an effort to predict the overall lactone conformation and steric environment of the quinoline chain, it was necessary to obtain more information about the spatial proximity of proton pairs in solution (Figure S2). A spatial proximity map was built from the observed NOEs found in 2D phase sensitive ^{1}H NOESY (Table 3). The intra-lactone interactions of

Table 2. Experimental and Calculated Coupling Constants Corresponding to Some Torsion Angles of Structures[a] **S** Computed for RU 004 by MD

		NMR		J_{calc} MD					X-ray	
vicinal pairs	J_{exp} D_2O	CD_3OD	$CDCl_3$	**S2**	**S3**	**S7**	**S11**	**S20**	$\mathbf{S}^+$	$\mathbf{S}^-$
H4−H5	8.2	8.7	8.6	10.9	11.0	11.0	11.0	3.6	11.0	11.1
H5−C3			3.0	2.8	2.7	2.7	2.7	5.6	2.7	2.5
H5−Me6			1.2	1.8	1.5	1.7	1.9	1.8	1.8	1.8
H7a−H8		9.0	12.3	12.4	12.3	12.4	12.4	12.4	12.4	12.4
H7b−H8		5.2	2.0	2.3	3.2	2.5	2.5	2.2	2.4	2.4
H10−H11	1.5	1.5	1.5	1.9	1.7	1.9	2.0	2.1	1.9	1.9
H11−Me12			0.8	1.0	1.9	1.0	1.0	0.8	0.9	1.0
H11−C16			3.7	3.9	2.6	3.9	3.9	4.0	3.9	3.7
H13−H14a	9.9	10.5	10.7	12.3	12.2	2.3	12.3	12.3	12.3	12.3
H13−H14b	2.4	2.3	2.1	2.3	2.2	12.4	2.3	2.3	2.4	2.4
ψ_1 H5−C1′			6.2	5.4	5.4	5.4	4.8	4.6	5.4	5.5
ψ_2 H1′−C5			2.0	2.2	1.8	2.2	5.4	2.6	2.3	2.3
17NH−H17A			2.5	5.3	4.5	5.3	5.5	6.4	5.3	5.1
17NH−H17B			4.5	4.5	5.3	4.5	4.5	3.6	4.5	4.8

[a] **S** structures have been defined according to notation in Table 5: **S2**: **M1D1T1C2**; **S3**: **M1D1T1C3**; **S7**: **M1D1T2C2**; **S11**: **M1D3T1C2**; **S20**: **M2D2T1C2**; X-ray $\mathbf{S}^+$: **M1D1T1**; X-ray $\mathbf{S}^-$: **M1D1T1**.

[10]7, [11]6-OMe, [11]7, [12-Me]2, [12-Me]10, [13]6-OMe (D2O−DMSO) and [15-Me]2-Me NOEs in solution are indicative of the close cross-ring proximity of these protons in the conformation **M1** (Table 3). This major conformer was characterized (Figure 2) by the "up" position of the three carbonyl groups (1-CO, 3-CO, and 9-CO). The conformation **M2** is present when the 3-CO group resides in an "exo" orientation with respect to the macrocycle (Figure 2a) and is defined by the observed NOEs [6-OMe]4, [12-Me]4 and especially [11]4 (Table 3).

For the orientation of the ethyl unit in RU 004, the [15-Me]2-Me NOE (Table 3) suggest that the position of this unit is relatively restrained and corresponds to a major parallel orientation **T1**, as for 6-OMe-roxithromycin or clarithromycin.

The five stacking conformers of the quinoline chain (Figure 3a) depend on whether the aromatic nucleus is found, and the observed [17]6-OMe, [17]11, [17]13, [17-NH]10-Me, [21]6-OMe, [22]6-OMe, [24]2-Me, [26]15-Me, [27]13, and [27]15-Me NOEs (Table 3) are indicative of a **C2** conformation where the quinoline plane resides above the 1-CO group (Figure 3a). The major observed NOEs ([24]2-Me, [26]15-Me, [27]13, and [27]15-Me) are unlikely to be indicative of the other conformers, on the basis of molecular modeling calculations. Additional NOEs [18]11, [18]13, [19]6-OMe, [21]15-Me, and [22]-15-Me are due to a different position of the aromatic nucleus and cannot be resolved from $\mathbf{S}^+$ **C1**−**C6** NOEs (Figure S2). They could be extrapolated from the additional $\mathbf{S}^-$ structures with **C1**- and **C2**-chain conformations (Figure S2).

A comparison of the NOEs in $CDCl_3$, CD_3OD, and D_2O−DMSO solution (Tables 3 and S3) shows that some **C2** characteristic proximities ([22]6-OMe, [24]2-Me, [26]2-Me, [27]13, and [27]15-Me) were no longer observed in this solvent. These weaker interactions indicated a possible reorganization of the quinoline chain in D_2O and suggest a **C3** conformation of the chain above the 6-OMe group (Figure S2).

If we analyze the amplitude of the movement of the quinoline chain, the NOESY NMR experiments demonstrated all the spatial proximities characterizing the **C2** conformation in the structures $\mathbf{S}^+$ and ones assigned to the **C1**-chain conformation in $\mathbf{S}^-$ structures (Figure 5b). The quinoline chain **C2**-(+) is stopped at the right-hand side by the 6-OMe group and is held between 1-CO and 3-CO ending up above 3-CO, while the **C1**-(−) chain of RU 004 is pushed back toward the left part of the macrocycle in the C(11)−C(13) region (Figure 5b). The end of the quinoline chain in the **C2** structure was close to the contact region of the sugar unit.

Additionally, the NOE data (Table 3) predict the orientation of the sugar ring with respect to the lactone ring. Few contacts between erythronolide and desos-

Table 3. Observed NOEs[a] for RU 004 in D_2O−DMSO (20:80, 4 mM) Solution. Interproton Distances[b] from Minimized Structures Derived from MD

observed NOEs	connectivities[c]			
	Intramacrocycle			
	M1	**M2**	**M3**	**M4**
10−7a	**p**	**p**		**p**
10−7b	**p**	**p**		**p**
10−8Me	**p**	**p**		
11−4		**p**		
11−6OMe	**p**	**p**	**p**	
11−7b	**p**	**p**	**p**	
11−8			**p**	**p**
12Me-4		**p**		
12Me-10Me	**p**	**p**		**p**
13−6OMe	**p**	**p**	**p**	
13−10				**p**
	T1	**T2**	**T3**	
15Me-2Me	**p**		**p**	
15Me-12Me		**p**	**p**	
	Desosamine Macrocycle			
	D1	**D2**	**D3**	**D4**
1′-4Me	**p**	**p**	**p**	**p**
1′-6Me	**p**		**p**	
2′-6Me	**p**	**p**		**p**
5′-5	**p**	**p**		
	Macrocycle-Chain			
	C1	**C2**	**C3**	**C6**
17−6OMe		**p**	**p**	
17−11	*p*	**p**	**p**	
17−13	*p*	**p**	p	
7NH-10Me	*p*	**p**	p	p
18−6OMe	*p*	**p**	p	
18−11	*p*	**p**		
18−13	*p*			
19−6OMe	*p*			
21−6OMe		**p**	*p*	
26−15Me		p		

[a] Some evident contacts intra-unit found for the different structures are not specified. [b] 2−4 Å. [c] p: present [**p** ($\mathbf{S}^+$, $\mathbf{S}^-$), p ($\mathbf{S}^+$), and *p* ($\mathbf{S}^-$)].

Table 4. Simulations of 200 ps at 300 K with Dielectric Constant $\epsilon = 4r$ Starting from the S^+ X-ray Structure and Six Arbitrary Conformations Representing Various Families[a]

		starting S^+ conformations (frequency)								
family	S^+	conformation	**S2** (X-ray)	**S3**	**S7**	**S11**	**S16**	**S20**	**S23**[b]	total frequency
S_I	**S1**	**M1D1T1C1**								
	S2	**M1D1T1C2**	x (149)	x (166)	x (187)	x (167)	x (184)	x (180)		1033 86
	S3	**M1D1T1C3**	x (1)							1
	S4	**M1D1T1C4**								
	S5	**M1D1T1C5**								
	S6	**M1D1T2C1**								
	S7	**M1D1T2C2**	x (39)	x (26)		x (7)	x (14)	x (8)		94 8
	S8	**M1D1T2C3**	x (1)	x (1)						2
	S9	**M1D1T2C4**								
	S10	**M1D1T3C1**								
S_{II}	**S11**	**M1D3T1C2**			x (8)	x (22)		x (9)		39 3
	S12	**M1D3T1C3**								
	S13	**M1D3T1C4**								
	S14	**M1D3T2C2**		x (2)						2
	S15	**M1D3T2C5**								
S_{III}	**S16**	**M1D4T1C2**	x (1)	x (1)	x (3)					5
	S17	**M1D4T1C3**								
	S18	**M1D4T1C4**								
S_{IV}	**S19**	**M2D2T1C1**								
	S20	**M2D2T1C2**	x (4)	x (4)	x (2)	x (4)	x (2)	x (3)		19 2
	S21	**M2D2T1C3**								
	S22	**M2D2T2C2**	x (5)							5
S_V	**S23**	**M3D1T1C3**							x (154)	
S_{VI}	**S24**	**M4D1T1C6**							x (46)	

[a] Each column represents one simulation and x indicates that conformation was found. The frequency is the number of times each conformation was found. [b] The two structures of high energy (**S23** and **S24**) were exceptionally generated by a protocol using temperature jumps at 800 K and starting from one S^- structure built using the INSIGHT II builder module. At 300 K, during 200 ps no interconversion was observed from S^+ to S^- structures. Therefore, they are never generated during 1200 ps, at 300 K.

amine are conserved for RU 004, attesting to some mobility. The sugar-lactone NOE from H(1′), [1′]5 cannot be observed because of overlapping, just as [2′]7 is indiscernible from [4]7. These observations suggest that the desosamine may fluctuate between relatively close positions (**D1**−**D3**) (Table 3). The set of $^3J_{^{13}C-^1H}$ coupling constants (Table 2) and the pattern of sugar-lactone NOEs [1′]4-Me, [5′]5, and [5′-Me]5 in solution suggest that the position of this unit is relatively restrained or corresponds to a major perpendicular orientation **D1** (Figure 4).

Part 2. Molecular Modeling. A pictorial representation of the solution conformation of RU 004 was obtained through computational chemical methods (molecular dynamics and molecular mechanics calculations), starting first with the two X-ray structures of RU 004 supplied by Hoechst Marion Roussel laboratories since the data are not available through the Cambridge Crystallographic Database (Figure 5a).

A second minimization was performed from an initial structure arbitrarily built with the quinoline chain modeled on the 3-keto 6-methoxy erythromycin. Upon direct minimization, a much lower energy structure S^- was obtained, even if, in practice, it does not contribute measurably.

Third calculations were performed with distance constraints based on the observed TRNOE data. At last, minimization was performed, releasing all constraints.

The aims of this work are to use MD calculations (i) to determine the rotational freedom about the endocyclic dihedral angles in the macrocycle **M** and thus, on the basis of the minimum energy level of **M** conformation, to generate the approximate ratios of minimum-energy conformations available up to 1−3 kcal mol^{-1}, (ii) to determine the flexibility of the desosamine **D** about the glycosidic bond joining the sugar to the lactone ring and predict the available conformational space for desosamine, and (iii) to determine the conformational freedom of the quinoline moiety **C**.

The structures found to have more energy up to 10 kcal mol^{-1} will be representative of very hindered intermediates.

The conformational analysis was carried out using the MD method in order to perform a more extensive study on the ketolide system whose conformations could be analyzed experimentally. RU 004 is a molecule with a moderately large conformational space and a computationally manageable size. RU 004 has the advantage of not presenting a hydrogen bond network as observed for erythromycin or roxithromycin due to their free OH-(6), OH(11), and OH(12) hydroxyl groups. Thus, there is hope that the results from simulations using a distance-dependent dielectric constant ($\epsilon = 4r$)[35] in the absence of explicit solvent might have relevance to the results in solution.

MD Protocols. All the simulations were carried out by using the DISCOVER program of BIOSYM package with the CVFF force field from Dauber-Augusthorpe and Hagler.[36] The above calculations presumed the default value of $\epsilon = 4r$ for the local dielectric constant,[35] a reasonable analogy for the solvent. There remains, however, the uncertainty regarding a parameter considering or ignoring the rotational entropy of the aromatic nucleus of the quinoline side chain. The short periods at 600 K were incorporated in order to prevent staying in the same local energy gap and to help jump over eventual barriers by increasing the kinetic energy in order to identify the global energy minimum.[37] When the MD sampling efficiency is low, the method of multiple starting points may help to improve the result (Table 4).[38] Starting from different conformations in order to better sample phase space seems more efficient

Table 5. Energy and Torsion Angles Computed for Structure Families of RU 004[a] Represented by 24 Low-Energy Conformations

family (%)	structures S^+, S^-	conformation	H4−H5	H8−C10	H11−Me12	ψ_1	ψ_2	S^+ E_p	S^+ P_i	S^- E_p	S^- P_i
S_I (95−97)			165	160	−100	10	55				
	S1	**M1D1T1C1**								193.0	22
	S2	**M1D1T1C2**					86	192.3	86	193.8	38
	S3	**M1D1T1C3**						196.3	0.5	196.5	9
	S4	**M1D1T1C4**								197.0	18
	S5	**M1D1T1C5**								197.1	2
	S6	**M1D1T2C1**								194.3	2
	S7	**M1D1T2C2**					8	194.2	8	195.5	2
	S8	**M1D1T2C3**						196.7		197.6	0.5
	S9	**M1D1T2C4**								197.8	3
	S10	**M1D1T3C2**								199.1	
S_{II} (1−3)			165	160	−100	−20	−10				
	S11	**M1D3T1C2**						194.9	3	196.7	1
	S12	**M1D3T1C3**								199.8	
	S13	**M1D3T1C4**								199.1	
	S14	**M1D3T2C2**								198.1	
	S15	**M1D3T2C5**								202.7	
S_{III} (0.5)			165	160	−100	15	145				
	S16	**M1D4T1C2**						196.3	0.5	197.6	0.5
	S17	**M1D4T1C3**								200.1	
	S18	**M1D4T1C4**								200.5	
S_{IV} (2)			120	175	−100	23	50				
	S19	**M2D2T1C1**								197.5	0.5
	S20	**M2D2T1C2**						195.3	2	196.9	0.5
	S21	**M2D2T1C3**								201.0	
	S22	**M2D2T2C2**						197.3		197.8	1
S_V (0)			180	10	−100	10	55				
	S23	**M3D1T1C3**						203.6			
S_{VI} (0)			−170	−40	−160	10	55				
	S24	**M4D1T1C6**						207.9			

[a] The two structures of high energy (**S23** and **S24**) were exceptionally generated by a protocol using temperature jumps at 800 K and starting from one S^- structure built using the INSIGHT II builder module. At 300 K during 200 ps, no interconversion was observed from S^+ to S^- structures. Therefore, they are never generated during 1400 ps, at 300 K.

than a very long MD run since choosing the right starting structure is likely to be crucial there.[38] For example, when structure **S23**$^+$ was used as the starting structure for a 200 ps MD run (Table 4), only the highest energy molecules, **S23**$^+$ (154) and **S24**$^+$ (46) were found. This result was able to bias further conclusions and thus was not included in the total frequency.

We have run dynamics, starting from each of the two (S^+) and (S^-) conformer families (Figure 5a), and different lowest energy conformations were then used as starting structures for the next 200 ps MD run at 300 K which totalled a 1400 ps simulation, respectively (Tables 4 and S5). For all of the dynamic experiments considered, no interconversion between the (S^+) and (S^-) families was observed at less than 600 K. Only at 800 K, with $\epsilon = 78$, was an interconversion observed, the **S5**$^-$ conformer with a nonstacking chain leading to the **S23**$^+$ and **S24**$^+$ conformers with energy about 10 kcal mol^{-1} above the minimum of the **S2**$^+$ conformer. Conversely, the S^+ structures are stable during this protocol. It seems that there is a high energetic barrier between the two families. The equilibrium is governed by complex interactions between the aromatic nucleus of the quinoline chain and the macrolactone ring. These interactions are particularly marked in the conformations which bring the π electrons or the nitrogen of the quinoline close to the 3-carboxy and 6-OMe groups.

At each protocol, the energies and the theoretical NMR data from the different (S^+) and (S^-) conformers were compared (Tables 2, 5, and S3). The 24 lowest energy conformations resulting from this study are listed in Table 5 and shown in Figures S3 and S4 of the Supporting Information. All of the conformers will later be referred to by the names in this Table. The global minimum was found in the very first trial, and the lowest energy conformations were found to be **S2**$^+$ (192.3 kcal mol^{-1}) and **S1**$^-$ (193.0 kcal mol^{-1}) (Figure 5b). In all cases, S^+ conformers are obtained with energies (1−2 kcal mol^{-1}) lower than those of the corresponding S^- ones.

This detailed analysis using variable-temperature molecular modeling experiments indicated that RU 004 exists in equilibrium with different macrolide conformations (Figure 6).

Structural Families. Conformational similarities were evaluated by calculating the root mean square index of deviation between heavy atoms after superimposition. Small rms deviations (<0.5 Å) for certain groups of structures suggest that they may belong to the same conformational family. As can be seen in Table 5, six families (S_I−S_{VI}) were found this time.

The S_I structure family corresponds to conformation **M1D1** involving a macrocycle conformation **M1** and a sugar ring **D1** with an orientation nearly perpendicular to the macrocyclic lactone ring. The ratio of S_I (**S1**−**S10**) family (97%) observed statistically during a 1200-ps dynamics protocol agrees well with the ratio calculated (90%) by the Boltzmann distribution of (**S1**−**S10**). MD generates conformations according to their probability of occurrence at equilibrium, provided that the simulation time is long enough.

Comparison between NMR and MD Data. The final structures obtained after several such calculations were examined for the overall energetic favorability and compared with the structures derived from the NMR data. Tables 2 and S3 compare the NMR and MD data.

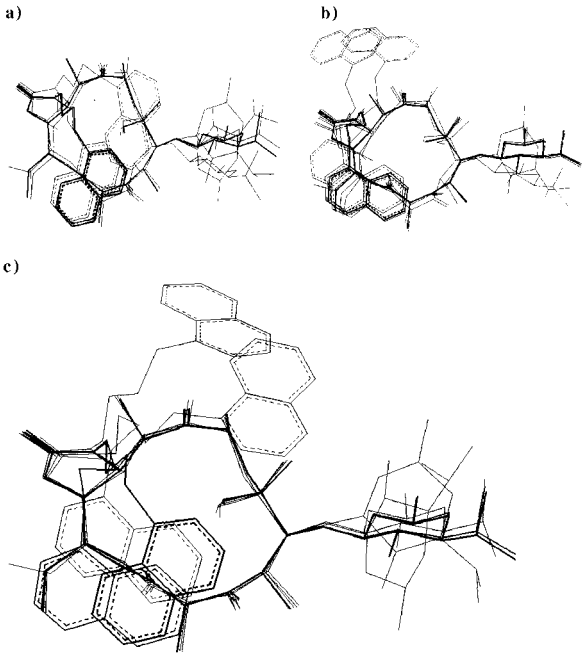

Figure 6. Conformational space can be well represented by a few well-defined conformers: (a) the predominant **S2**$^+$ in bold and the minor **S**$^+$ ones (**S3**$^+$, **S7**$^+$, **S11**$^+$, **S16**$^+$, and **S20**$^+$); (b) the predominant **S1**$^-$ in bold and the minor **S**$^-$ ones (**S4**$^-$, **S5**$^-$, **S6**$^-$, **S13**$^-$, and **S19**$^-$); and (c) conformational averaging for RU 004 in solution (**S**$^+$ and **S**$^-$ structures).

For each conformation obtained from MD, coupling constants $^3J_{H,H}$ and $^3J_{C,H}$ are estimated using Karplus-type equations[31,32] and are compared to the observed vicinal coupling constants. A comparison between experimental (NMR) and calculated coupling constant values obtained in MD simulation is made to estimate eventual conformational equilibrium.

The similarity between the geometry in solution and that of several MD conformers was also investigated from the intensive NOESY correlations observed. The spatial proximity values computed from the low-energy structures having macrocycle, chain, and sugar in different conformations will be compared with the observed NOE values in Table 3.

During the MD simulation, the minor structures were in conformational averaging with a major participation of the more stable conformer **S2**$^+$. The predominant **M1D1T1** conformation determined from the theoretical MD structures is in agreement with the preponderant experimental NMR results in solution. It is concluded that RU 004 exists in solution as one major conformer very similar to the more stable conformer **S2**$^+$ (Figure 5b). Thus, after finding conformations, one needs to produce an effective ensemble in which all of the most significant conformers have been located (Figure 6). Other minor conformation **S**$^+$ (Figure 6a) and **S**$^-$ (Figure 6b) participate a little bit in solution (Figure 6c). In conclusion, MD experiments are of great benefit in predicting the specific range of minor conformations available in solution.

Comparison of RU 004 with Other 14-Membered-Ring Macrolides. The solution structure of RU 004 is compared to the solution structures of 6-OMe-roxithromycin and clarithromycin. Slight deviations are noted for RU 004 concerning the values of heteronuclear ^3J coupling constants in the lactone ring, [$^3J_{H(5)C(Me6)}$ (1.2 Hz), $^3J_{H(5)C(3)}$ (3.0 Hz)] compared with those of 6-OMe-roxithromycin [$^3J_{H(5)C(Me6)}$ (3.0 Hz), $^3J_{H(5)C(3)}$ (4.6 Hz)] and clarithromycin [$^3J_{H(5)C(Me6)}$ (3.1 Hz), $^3J_{H(5)C(3)}$ (3.6 Hz)]. This could be related to a different position or motion of the carbonyl at C(3) and/or the desosamine moiety bonded at C(5) and/or the methyl group bonded at C(4) and/or the steric effect of the quinoline chain above the macrocycle as well as the bulky OMe-6 group pointing up.

The two conformations of RU 004, **M1** with the 3-CO carbonyl group in a position "up" above the macrocycle and **M2** with this group in an "exo" orientation (Figure 2) might be compared to the two types of conformation found in erythromycin derivatives. In erythromycin A (ketone form) solution, the macrocycle is mainly found in the C(3)−C(5) folded-out A conformation but in conformational equilibrium with the minor folded-in B conformation with the cladinose unit rising above the macrocycle.[39,40] While its ketal metabolite always present the inward folding C(3) fragment, the B macrocycle in which the sugar moiety is tilted up.[40] In a solution of roxithromycin derivatives, the macrocyclic lactone ring corresponds to the C(3) fragment folded-out and conformation A with the desosamine sugar is found to be essentially perpendicular to the macrocycle (**D1** conformer).

The 6-OMe group, the 11,12-five cyclic hydrazono-carbamate and the quinoline side chain strengthen the rigidification of the erythronolide region C(6)−C(12). Consequently, the degree of movement of desosamine sugar increases in the following ways. The MD study of RU 004 clearly demonstrated that the ketolide desosamine ring had more conformational freedom (**D1**−**D4**) than in clarithromycin, roxithromycin, or 6-OMe-roxithromycin.

An interesting feature of RU 004 has been revealed by the NMR and MD data. In the **S2**$^+$ structure, the 4-methyl group is situated in a part of the space normally occupied by the cladinose sugar. Moreover, the quinoline moiety (**C2**) overlaps the macrolactone ring above the two carbonyl 1-CO and 3-CO groups. The chain is also enclosed between the 6-OMe group at the right and the 11,12-five cycle at the left part of the macrocycle and consequently loses some of its mobility.

The replacement of the cladinose sugar by the 3-keto function and the prevention of 6, 9−9, 12 cyclization are likely to be unequivocally advantageous since this increases hydrophobicity of RU 004 when compared with that of clarithromycin, roxithromycin, or 6-OMe-roxithromycin. That will give rise to different, perhaps complementary, pharmacokinetic properties.

Part 3. TRNOE Experiments. It has been shown that roxithromycin, erythromycin A (the 9-keto form), and their 6-*O*-methyl derivatives bind in fast exchange on the NMR time scale to bacterial ribosomes, the drug target, whereas metabolites derived from them by an acidic cleavage of the cladinose sugar do not bind to bacterial ribosomes and do not exert antibiotic activity.[13,14,19,30] Taking advantage of the exchange between bound and free macrolide antibiotic, we have developed a study of the ketolide−ribosome interactions of RU 004 to *Escherichia coli* ribosomes, using 2D transferred nuclear Overhauser effect spectroscopy (TRNOESY).

Composition of the Binding Buffer. The weak interaction between macrolide antibiotics and ribosomes observed by NMR[14] was found to be Mg^{2+} independent {the experiments were performed with roxithromycin in various phosphate buffers at apparent physiological pH 7.6, potassium phosphate buffer 50 mM with KCl 200 mM and $MgCl_2$ 10 mM, potassium phosphate buffer 50 mM with KCl 200 mM, and TRIS buffer 10 mM with NH_4Cl 10 mM}, but the tight interaction measured by the binding test between macrolides and *E. coli* ribosomes is strongly Mg^{2+} dependent.[41] It is known that cations are essential for macrolide−ribosome interaction[17,42] and [^{14}C]erythromycin binding is negligible in the absence of K^+ and is almost optimal at 100 mM. The high K^+ concentration (200 mM) is used in this study to improve a better ribosome stability (same result with KCl 0.1 M as 0.2 M). Although a minimal concentration of Mg^{2+} is required for optimal binding, at 0.1 mM Mg^{2+} substantial [^{14}C]erythromycin binding to ribosomes is observed. Magnesium ions are also involved in ribosomal subunit association and its stabilization.[43,44]

The experiments were performed with RU 004 in phosphate buffers at apparent physiological pH 7.6. The antibiotic samples were dissolved in an aqueous NaD_2PO_4−Na_2DPO_4 buffer (0.05 M) with KCl (0.2 M). Physical parameters of crucial importance for chemical exchange such as temperature, substrate-ligand ratio, and *E. coli* ribosomal concentration have to be optimized.[14]

Ketolide−Ribosome Ratio. The line-broadening of RU 004 is proportional to the amount of ribosome. With 0.8 μM concentration of ribosomes as for the other macrolides, the line-broadening was then too large to allow ligand signals to be detected. Low ribosomal concentration (0.16 μM) with a larger fraction of ligand (2 mM) causes half line-broadening of the RU 004 signals as well as TRNOE cross-peaks clearly observable. Assuming that the correlation time of the interproton vector motion (τc) increases in proportion to the molecular mass of the complex, the TRNOEs would be observable even for a large excess of ligand (e.g., a 5000:1 ratio for 14-membered-ring macrolides).[45] Here, with a 12500 ligand−ribosome ratio, transferred NOE effects from ketolide−ribosome interactions can be observed only with such concentrations. This result suggested that chemical exchange for ketolides is slower than that for previously studied macrolides.[13,14,30]

Temperature Effect. We have investigated the effect of temperature on the exchange with 0.8 μM ribosomal concentration and with 0.2 mM fraction of ligand. One experimental way to distinguish between slow and fast exchange (relative to T_2^B the relaxation time of the bound nuclei) is to measure the temperature dependence of the line width of the exchanging nuclei.[46] If there is no chemical shift difference between the two states (free and bound), the observed relaxation rate $1/T_2^{obs}$ is described by the relationship

$$\frac{1}{T_2^{obs}} = \frac{1}{T_2^F} + \frac{p_B}{T_2^B + \tau_B}$$

where T_2^F is the spin−spin relaxation time of the free nuclei, p_B the fraction of macrolide in the bound state, and τ_B the exchange lifetime of the bound macrolide. The exchange rate, $k_{-1} = 1/\tau_B$ will increase with temperature. In the slow exchange limit ($T_2^B \ll \tau_B$), the line width ($1/\pi T_2^*$) will increase with temperature. For fast exchange ($T_2^B \gg \tau_B$) on the other hand, the opposite situation prevails, and the resonance lines will narrow with increasing temperature.

Fast exchange seems to prevail for macrolide−ribosome interaction as the resonance narrows with increasing temperature. The situation is quite different for RU 004−ribosome interaction. At 280 K, in the presence of 0.8 μM concentration of ribosomes in buffered D_2O solution, the resonance lines of RU 004 (0.2 mM or 2 mM) are sharp. As the temperature is increased to 293 K, signals of RU 004 are very large and hardly observable, and they widen with increasing temperature until they disappear at 313 K.

Another parameter has to be refined, the TRNOEs time dependence of RU 004 (τ_m < 50 ms) to avoid spin diffusion. Indeed, spin diffusion effects appeared for mixing times larger than 150 ms for macrolides.

Bound Conformation. This compound exists in solution in one predominant conformation. The TRNOEs NMR experiments suggest that it binds in its receptor site in essentially the same conformation as that which exists free in aqueous solution. The TRNOESY spectra of RU 004 contain 95 cross-peaks which were due to spatially proximate hydrogens in the free drug.

The bound ketone structure of RU 004 is blocked into a specific and privileged conformation in weak interaction with *E. coli* ribosomes. In particular, NOEs relative to the **M1D1T1** conformation appear strongly with ribosomes. A comparison of free and bound structures of RU 004 shows that the bound conformation of RU 004 participated in the conformational averaging in D_2O solution. The main differences are the missing NOEs, namely [8-H]6-OMe, [11-H]4-H, [11-H]7-H, [11-H]8-H, [12-Me]4-H, [13-H]10-H, and [13-H]2-Me, which were due to a minor presence in solution of **M2** and **M3** erythronolide ring conformations. At the same time, the NOEs [14-H]2-Me and [15-Me]2-Me indicate that the ethyl group of the macrocycle is directed essentially toward the 2-Me group (**T1**) when the TRNOEs [11-H]6-OMe, [12-Me]8-Me, and [15-Me]2-Me correspond to a similar conformation **M1** of the macrocyclic ring in ribosomal solution.

The observed TRNOEs are compared to the spatial proximity values computed from the low-energy conformers having sugars in **D1**−**D4** positions (Figure 4). The desosamine−lactone NOEs [5-H]1′-H, [5-H]5′-H, [4-Me]1′-H, [6-Me]1′-H, and [6-Me]2′-H are those expected if the sugar ring is oriented approximately perpendicular to the macrocycle lactone ring with 5′-Me pointing up (**D1**). The lack of the NOEs [7-H]1′-H and [6-Me]5′-H characteristic of the **D3** conformation indicated that in bound conformation the distance between these groups is greater than 4 Å. As evidenced from the constraints of the different TRNOEs observed in buffered D_2O, the relative rigidity of the sugar unit in ketolide−ribosome complex seems to be confirmed.

For RU 004, the TRNOEs NMR experiments at 50 ms demonstrates the spatial proximity of 6-OMe to 11-H, 21-H, 27-H, and 25-H. At the same time, the lack of

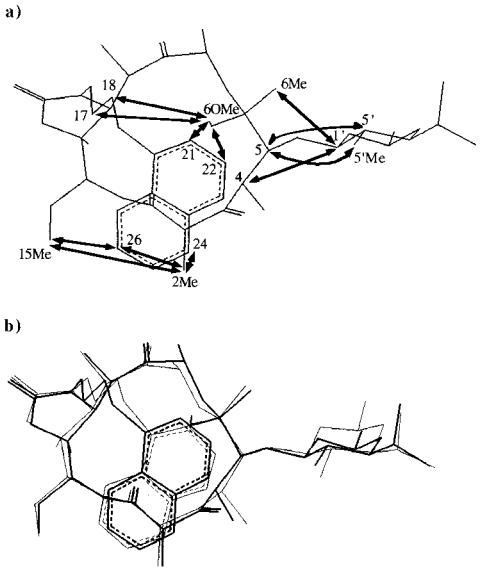

Figure 7. (a) Some characteristic TRNOEs for the bound RU 004 structure. (b) Superimposition of the **S2**$^+$ conformation generated by the MD- and TRNOESY-derived structure, weakly bound to bacterial ribosomes for RU 004. The quality of superimposition of all the atoms was evaluated by root mean square (rms) deviation between the atoms constituting the bound conformer in bold and the corresponding atoms in the **S2**$^+$ conformation (rms, 0.3928 Å).

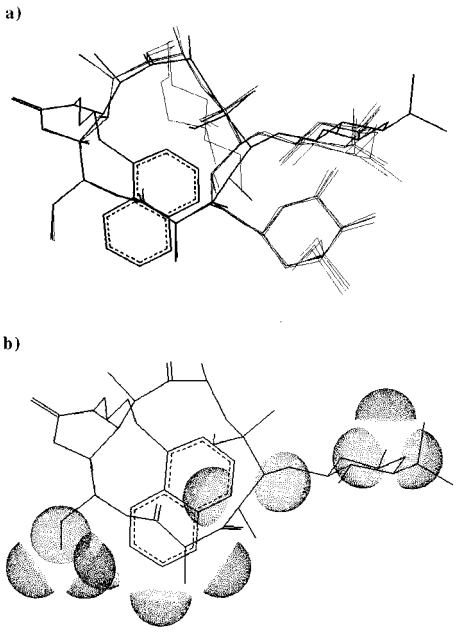

Figure 8. (a) Superimposition of RU 004, roxithromycin, 6-methoxy-roxithromycin, erythromycin, and clarithromycin TRNOESY-derived structures, weakly bound to bacterial ribosomes (rms, 0.8709 Å). (b) Minimized structure from transferred NOEs data (bound to ribosomes) of RU 004. The van der Waals surfaces are shown to indicate the atoms whose signals are most broadened (15-Me, 5′-Me, 4-H, 5-H, 24-H, 25-H, and 26-H). The broadening observed may reflect proximity to a binding surface.

the NOEs [17-H]13-H, [18-H]11-H, [18-H]13-H, [22-H]-15-Me, [27-H]13-H, and [27-H]15-Me shows that the quinoline chain is displaced toward the right-hand side (6-C) of the molecule rather than toward the C(13)−C(15) region (Figure 7a). The bound structure shows a slight distortion of the **C2** quinoline chain conformation in a structure **S**$^+$. The quinoline chain is holding toward 3-CO, spatially proximate to 6-OMe and finally ends close to the part of the desosamine sugar joined to the macrocycle (Figure 7b).

Binding Surface. In general, a correlation between line broadening and involvement in binding is expected. Line broadening in NMR spectra may result from two distinct processes, equilibrium between states with different chemical shifts and slowing of molecular motion. Macrolides bind to ribosomes at an identical surface of the drug molecule to erythromycin A, involving the C(13)−C(5) lactone region of the aglycone and both sugar rings, essentially the cladinose.

Finally, a model of RU 004 showing the hydrogen atom giving the most extensively broadened resonances is constructed (Figure 8b) using van der Waals surfaces. The model is based on the minimized structure derived from MD experiments and will be compared to the ones suggested for clarithromycin and for roxithromycin.[13,14,30] The surface of RU 004 deduced from the variation in line broadening would be indicative of the relatively rigid part of the molecule. However, it is not initially exact for the free molecules. The data corresponding to the C(4)−C(5) region are indicative of near-rigid rotation of these atoms in close proximity to the ribosome due either to a sterically hindered rotation or to specific interunit (ribosome−ketolide) bonds involving this region, while conformational instability appears in the C(3)−C(5) region of the free antibiotics in the molecular modeling study. In the free ligand, this portion of macrocyclic ring can fold inward so that the 3-CO group pushes out the macrolactone leading to the **M2** conformation.

From these experiments, the **M1D1T1** conformation (similar to **S2**$^+$) appears to be the plausible bound structure relative to this weak specific binding to the bacterial ribosome, and the broadening observed in the C(13)−O(14)−C(2)−C(4), C(24)−C(26), and C(5′-Me) region may reflect proximity to a binding surface.

The structures representing the bound state of the drugs (RU 004, erythromycin, clarithromycin, roxithromycin, and 6OMe-roxithromycin) show conformational homology after superimposition (Figure 8a): the C(13)−O(1)−C(1) region is almost completely superimposable with variation in the right-hand side of the molecule. Superimposition of the bound structures revealed one change that may be of importance for the ketolide mode of action, a stretching out of the desosamine dimethyl amino group. The flexible right-hand side of the macrolide ring C(2)−C(5) exhibits some deviation from clarithromycin and roxithromycin, thus the position of the desosamine sugar is not exactly the same in the ketolide as in other drugs. The dimethyl amino group of RU 004 has moved by ca. 1.5 Å away from the C(13)−C(15) region (Figure 8a).

Unlike the effects the oxime chain above the macrocycle for roxithromycin and 6OMe-roxithromycin found in the previous studies by TRNOEs NMR experiments,[30] it was the first time that a significant line broadening affected the chain moiety (H-24, H-25, and H-26) exactly in its external part close to the 1-CO−3-CO region. The broadening observed may reflect the proximity of the quinoline chain to a binding surface involving an additional interaction of ketolide with the ribosome. Whereas the line broadening affecting the cladinose

sugar of macrolides (erythromycin, clarithromycin, roxithromycin, and 6OMe-roxithromycin) may indicate a steric hindrance of this residue in macrolide−ribosome complex, this hindrance is removed in ketolides since the data suggest that the weakly bound state of RU 004 observed here is strengthened. This study can explain some of the significant differences between RU 004 and the other antibiotics.

Drug−Ribosome Interaction. The weakly bound state of the ketolide observed here probably represents a first stage in an allosteric two-stage binding process. The weak interaction and Mg^{2+} independence observed by NMR is in agreement with an hypothesis of two distinct binding levels, as was reported for ribosome−tetracycline interaction,[47] with a low affinity binding level and the tight inhibition binding one. This weak binding observed by TRNOE experiments could be involved in the first step of recognition and selection of macrolide antibiotics by the ribosomal machinery. Mg^{2+} could have a crucial role for the second tight stage. The divalent ion acts probably to strengthen macrolide binding and hence to inhibit protein biosynthesis by macrolide antibiotics. Thus, Mg^{2+} does not play a direct role for the low affinity binding site studied by TRNOE. It is possible that Mg^{2+} may form a connecting bridge between the drug and the ribosome. Another possibility is that Mg^{2+} could maintain a tertiary structure necessary for the second step of interaction.

Compounds which are not able to take part in a weak binding interaction with bacterial ribosomes do not exert antibiotic activity[14] which was also observed by Barber et al.[18,48] Thus, the weak binding site seems to be a necessary step for the strong interaction. Unlike their parent compounds in vivo, roxithromycin and erythromycin A metabolites do not retain antimicrobial activity. Consequently, they are not able to take part in a binding interaction with bacterial ribosomes. These inactive metabolites showed very little line broadening and at the same time gave essentially blank TRNOESY spectra.[14]

To distinguish here between the specific effects of drugs binding to their targets and nonspecific interactions between small molecules and macromolecular complexes, ribosomal cores particles were prepared by incubating 50S subunits with 1.3 M LiCl solution to remove outer proteins.[49] Cores were used in place of whole ribosomes with RU 004 in control experiments. Spectra were run of RU 004 alone, in the presence of 0.16 μM ribosomes (a concentration determined to give a significant increase in line width of RU 004), and separately in the presence of 0.33 μM cores. The concentration of RU 004 was 2 mM, and the buffer solution in each case was potassium phosphate buffer 50 mM with KCl 200 mM. The addition of ribosomal cores to RU 004 resulted only in a slight broadening of all the lines in the control spectrum and a blank TRNOESY spectra. This indicates that the only interactions between RU 004 and ribosomal core particles are nonspecific and are typical of weak interactions between small molecules and large complexes. It was clear from these data that the active ketolide bound weakly to bacterial ribosomes in a similar way to erythromycin A group, as indicated by selective line broadening in the ^{1}H NMR spectra.

Conclusion

The NMR data indicate that although more than one conformer is present in solution, one conformer dominates [**M1D1T1C2** (**S2**$^+$)]. The set of proton−proton coupling constants and nuclear Overhauser effects as well as molecular modeling data yield a structure for the predominant conformer. A combination of NMR spectroscopy and molecular modeling techniques showed that the major solution state conformation is a 3-CO "up" type, while the contribution of the "exo" conformer in the solution is low but increases as the solvent is changed from $CDCl_3$ to more polar solvents. In summary, the data indicated that, in solution, the quinoline chain is anchored to the erythronolide above the two carbonyl 1-CO and 3-CO groups by electrostatic interactions.

The replacement of the cladinose sugar by the 3-keto function and the prevention of 6, 9; 9, 12 cyclization by the quinoline moiety overlapping the macrocycle combined with the various interactions increase the hydrophobicity of RU 004 when compared with that of clarithromycin or 6-OMe-roxithromycin. This should give rise to complementary, perhaps better, pharmacokinetic properties.

Here also, TRNOEs NMR experiments were proved to be efficient for the location and detection of the weak interactions due to ribosomal activity, providing a relationship between conformation in interaction and activity. Shifting of the desosamine dimethyl amino group, modification of C(4)−C(5) bond angle, absence of steric hindrance in the 3-keto area, and additional implication of the quinoline chain in the binding surface may be of importance for the ketolide mode of action. These results can explain some of the differences observed between RU 004 and 14-membered-ring macrolides (larger ratio, opposite temperature dependence, and spin diffusion effect). Thus, the ketolide exhibits higher affinity for weak ribosomal interaction than the macrolides.

The active molecule requires desosamine or a similar sugar at 5-C, and the 3-C sugar, proving not to be essential for antibacterial activity, may be replaced.[50]

The structural information (dihedral angles and spatial proximity) of the different conformations generated in this study would be of great benefit as references in predicting conformations in solution of new ketolide derivatives and the conformation in interaction with bacterial ribosomes.

Experimental Section

NMR Spectroscopy. The sample was dissolved in an aqueous NaD_2PO_4−Na_2DPO_4 buffer (0.05 M), with KCl (0.2 M) at physiological apparent pH 7.6 (pD = pH + 0.4, uncorrected here), and it was possible to attain concentrations of 0.5 mM for ^{1}H experiments. To improve its solubility in aqueous solution, we have to previously dissolved RU 004 in a minute amount of DMSO-d_6, and thus, we can attain concentrations of 2 mM.

A crystal of $TSPD_4$, 3-(trimethylsilyl)[2,2,3,3-d_4] propionic acid, sodium salt, was used as internal reference for the proton shifts. The errors on the chemical shifts are 0.01 ppm for ^{1}H.

The experiments were run at 500 MHz for ^{1}H, at 293 K, on Bruker AMX 500 spectrometers equipped with a Silicon Graphics workstation. A presaturation of the solvent was used for all the 1D and 2D ^{1}H experiments.

The 2D TOCSY spectra were recorded with data matrices of 2K × 256 points and processed using shifted sine bell squared window functions with zero filling in F_1 to 2K × 1K. The mixing time was 70 ms. The $^1H-^{13}C$ correlation spectra were recorded at 125.77 MHz with data matrices of 2K × 256 and processed using sine squared window functions with zero filling to 2K × 1K.

The 2D phase-sensitive using States-TPPI method ^1H TRNOESY experiments in D_2O buffered solution were performed using a mixing time from 25 to 800 ms. FIDs were acquired (64 scans) over 5555 Hz into a 2K data block for 256 incremental values of the evolution time and a relaxation delay of 2 s. Water suppression was performed by a low power transmitter pulse of presaturation (70 dB) during relaxation delay and mixing time. Two half-sinusoid (5% truncated) shape homospoil gradients of 10 G/cm were used before and after the mixing time, respectively.

Molecular Modeling. The calculations were run on a Silicon Graphics computer using the Biosym software INSIGHT II and DISCOVER with the CVFF force field from Dauber-Osguthorpe and Hagler.[36]

We have run experiments starting from the two different X-ray structures of RU 004. TRNOESY data were applied, and the following constraints were used: 3 ± 1 Å. The dynamics were run for 200 ps (constant temperature), and the trajectory was sampled by minimizing and storing the structure every ps.

First, the structures were built from the crystallographic coordinates of the solid RU 004 as a starting point. Their atomic potentials and charges were recalculated using the built-in algorithm of the program,[51] and the structures were modified into protonated molecules since they are bound to the bacterial ribosome at physiological pH 7.6. To take into account the polarization state of this molecule (the quinoline function presenting a 5.3 pK_A value is not protonated at physiological pH) and to check for eventual structural effects due to protonation of the dimethyl-amino group (at pH 7.6), the charges were recalculated[52] using the DISCOVER algorithm, with a total charge of +1. All calculations were performed, implicitly taking into account the effects of the solvent by using in the description of the Coulombic interaction a distance-dependent dielectric constant ($\epsilon = 4r$). The S^+ and S^- structures were generated from a preliminary exploration of the conformational space. After energy minimization and an equilibration period of 6 ps, we performed a 50 ps MD run at 300 K with periodic temperature jumps to 600 K to supply the system with energy (to pass conformational barriers). The 50 ps trajectory is sampled every ps and the remaining structures are then minimized by molecular mechanics and stored. The 24 final conformers found with lowest energies were then further minimized to a gradient less than 0.01 kcal/mol to obtain their energies at higher accuracy. Conformational similarities were evaluated by calculating the rms of deviation between heavy atoms for each possible pair of the different structures. The results represent the conformational averaging whose small rms deviations (<0.5 Å) suggested that they may belong to the same conformational $\mathbf{S_I}$ (**M1D1**) family.

Subsequently, RU 004 ($\mathbf{S}^-$) was modeled, and it did not appear to be inherently unstable. These data indicate the presence of a kinetic barrier to isomerization $\mathbf{S}^-$, $\mathbf{S}^+$. The initial structure was built starting with the X-ray crystal structure of erythromycin from the Cambridge Data Bank[53] with a 3-keto function in place of the cladinose moiety, a conversion of the 6-hydroxyl by a 6-methoxy group and removal conversion of the 11- and 12-hydroxyl groups by 11−12 cyclic hydrazono-carbamate carrying an alkyl-quinoline chain. The minimized conformation generated, **S13**, was then subjected to a 50 ps MD run with temperature jumps (300−600 K). After energy minimization and an equilibration period, the simulation was then continued for an 8 ps period at 300 K, followed by a temperature jump to 600 K during 4 ps. This alternation was repeated until a total simulation time of 50 ps was reached. The simulation was stopped every ps and the remaining structure energy-minimized using the previously described method. Repeating the above procedure in the simulations starting from nine different low conformations resulted in 450 structures generated during this process.

Second, two minimized conformations were then used as the starting structures of each $\mathbf{S}^+$ and $\mathbf{S}^-$ molecule for a 200 ps MD run, and TRNOESY data were applied. We can observe that, whatever the protocol was, the conformation **S2** was unique (100%). Upon beginning, the **S2** conformation is generated from these experiments.

The lowest energy-minimized constrained structure extracted from simulations was compared with the free **S2** major ligand for compound RU 004, using a superimposition procedure.

Ribosome Preparation. The ribosomes are prepared at Hoechst Marion Roussel as described[54] by a tangential ultrafiltration technique. The ribosomal purity is given by 1 unit A_{260} (absorption at 260 nm) which corresponds to 24 pmol ml^{-1} of 70S ribosomes. Microdialysis on Millipore membrane filters MF-type with 0.025-μm pore size was carried out beforehand to remove Tris impurities present during ribosome isolation. A concentration of 0.16 μM of *E. coli* MRE 600 strain 70S ribosomes is appropriate because it gives a 2-fold increase of the line width of RU 004.

50S core particles were prepared by incubating 50S subunits with 1.3 M LiCl solution. After precipitation by polyethylene glycol and centrifugation, microdialysis on Millipore membrane filters MF-type with 0.025-μm pore size was carried out beforehand with phosphate buffered solution for NMR to remove impurities. Core particles were frozen in nitrogen liquid and then stored at 193 K. The amount of cores is given by 1 unit A_{260} (absorption at 260 nm) which corresponds to 35 pmol ml^{-1} of 50S ribosomes.

Acknowledgment. This work was supported by grants from Hoechst Marion Roussel (Romainville Research, Medicinal Chemistry).

Supporting Information Available: Tables of experimental data and figures of conformational analytsis of RU 004 (11 pages). Ordering information is given on any current masthead page.

References

(1) Kirst, H. A. Macrolide Antibiotics. *Annu. Rep. Med. Chem.* **1990**, *25*, 119−128.
(2) Agouridas, C.; Bonnefoy, A.; Chantot, J. F. Ketolides, A New Distinct Semi-Synthetic Class of Macrolides: RU 004: *In Vivo* and *In Vitro* Antibacterial Activity. *34th Intersci. Conf. Antimicrob. Agents Chemother.* **1994**, F-168.
(3) Agouridas, C.; Benedetti, Y.; Denis, A.; Fromentin, C.; Gouin d'Ambrières, S.; Le Martret, O.; Chantot, J. F. Ketolides, A New Distinct Semi-Synthetic Class of Macrolides. *34th Intersci. Confer. Antimicrob. Agents Chemother.* 1994, F-164.
(4) Agouridas, C.; Benedetti, Y.; Denis, A.; Le Martret, O.; Chantot, J. F. Ketolides: A New Distinct Class of Macrolide Antibacterials. Synthesis and Structural Characteristics of RU 004. *35th Intersci. Conf. Antimicrob. Agents Chemother.* **1995**, F-157.
(5) Agouridas, C.; Bonnefoy, A.; Chantot, J. F. *In Vitro* Antibacterial Activity of RU 004, A Novel Ketolide Highly Active Against Respiratory Pathogens. *35th Intersci. Conf. Antimicrob. Agents Chemother.* **1995**, F-158.
(6) Ednie, L. M.; Spangler, S. K.; Jacobs, M. R.; Appelbaum, P. C. Susceptibilities of 228 Penicillin- and Erythromycin-Susceptible and -Resistant Pneumococci to RU 64004, a New Ketolide, Compared with Susceptibilities to 16 Other Agents. *Antimicrob. Agents Chemother.* **1997**, *41*, 1033−1036.
(7) Ednie, L. M.; Spangler, S. K.; Jacobs, M. R.; Appelbaum, P. C. Antianaerobic Activity of the Ketolide RU 64004 compared to Activities of Four Macrolides, Five β-Lactams, Clindamycin, and Metronidazole. *Antimicrob. Agents Chemother.* **1997**, *41*, 1037−1041.
(8) Jamjiam, C.; Biedenbach, D. J.; Jones, R. N. In Vitro Evaluation of a Novel Ketolide Antimicrobial Agent, RU-64004. *Antimicrob. Agents Chemother.* **1997**, *41*, 454−459.
(9) Cachet, T.; Van den Mooter, G.; Hauchecorne, R.; Vinckier, C.; Hoogmartens, J. Decomposition Kinetics of Erythromycin A in Acidic Aqueous Solutions. *Int. J. Pharm.* **1989**, *55*, 59−65.
(10) Delaforge, M.; Sartori, E.; Mansuy, D. In Vivo and In Vitro Affects of a New Macrolide Antibiotic Roxithromycin on Rat Liver Cytochrome P-450: Comparison with Troleandomycin and Erythromycin. *Chem. Biol. Interact.* **1988**, *68*, 179−188.

(11) Delaforge, M.; Sartori, E. In Vivo Effects of Erythromycin, Oleandomycin and Erythralosamine Derivatives on Hepatic Cytochrome P-450. *Biochem. Pharmacol.* **1990**, *40*, 223−228.
(12) Labbe, G.; Abbecassis, P. Y.; Courtin, O.; Flor, M.; Fougeat, S.; Bode, G. RU 004: A New Ketolide, *In Vitro* and *In Vivo* Effects on Hepatic Cytochrome P-450. *35th Intersci. Conf. Antimicrob. Agents Chemother.* **1995**, F-174.
(13) Bertho, G.; Ladam, P.; Gharbi-Benarous, J.; Delaforge, M.; Girault, J. P. Conformation of Macrolide Antibiotics Bound to Ribosome as Determined from Transferred Nuclear Overhauser Effect Spectroscopy. *J. Chim. Phys.* **1998**, *95*, 423−429.
(14) Bertho, G.; Gharbi-Benarous, J.; Ladam, P.; Delaforge, M.; Girault, J. P. Transferred Nuclear Overhauser Effect of Macrolide-Ribosome Interactions: Correlation between Antibiotic Activities and Bound Conformations. *Bioorg. Med. Chem.* **1998**, *6*, 209−221.
(15) Goldman, R. C.; Fesik, S. W.; Doran, C. C. Role of Protonated and Neutral Forms of Macrolides in Binding to Ribosomes from Gram-Positive and Gram-Negative Bacteria. *Antimicrob. Agents Chemother.* **1990**, *34*, 426−431.
(16) Fernandez-Munoz, R.; Vazquez, D. Quantitative Binding of ^{14}C−Erythromycin A to *E. coli* Ribosomes. *J. Antibiot.* **1973**, *26*, 107−108.
(17) Pestka, S. Binding of [^{14}C]Erythromycin to *Escherichia coli* Ribosomes. *Antimicrob. Agents Chemother.* **1974**, *6*, 474−478.
(18) Barber, J.; Gyi, J. I.; Pye, D. A. Specific, Weak Binding of Erythromycin-A (Ketone) and Chloramphenicol to 50S Subunits of *E. coli* Ribosomes − A ^{1}H NMR Study. *J. Chem. Soc., Chem. Commun.* **1991**, 1249−1252.
(19) Pye, D. A.; Gyi, J. I.; Barber, J. Tautomeric Recognition of Erythromycin A by Ribosomes − A^{1}H Nuclear Magnetic Resonance Study. *J. Chem. Soc., Chem. Commun.* **1990**, 1143−1145.
(20) Gyi, J. I.; Brennan, R. J.; Pye, D. A.; Barber, J. The Binding of Erythromycin A to Bacterial Ribosomes: A ^{1}H Transferred NOE Study. *J. Chem. Soc., Chem. Commun.* **1991**, 1471−1473.
(21) Agouridas, C.; Collette, P.; Mauvais, P.; Chantot, J. F. RU 004: Preliminary Studies on the Mechanism of Action. *35th Intersci. Conf. Antimicrob. Agents Chemother.* **1995**, F-170.
(22) Agouridas, C.; Collette, P.; Mauvais, P.; Chantot, J. F. Ketolides, A New Distinct Semi-Synthetic Class of Macrolides: RU 004: Preliminary Studies on the Mechanism of Action. *34th Intersci. Conf. Antimicrob. Agents Chemother.* **1994**, F-166.
(23) Bendall, M. R.; Pegg, D. T. Complete Accurate Editing of Decoupled Carbon-13 Spectra using DEPT and a Quaternary-only Sequence. *J. Magn. Reson.* **1983**, *53*, 272−296.
(24) Bax, A.; Summers, M. F. 1H and 13C Assignments from Sensitivity-Enhanced Detection of Heteronuclear Multiple-Bond Connectivity by 2D Multiple Quantum NMR. *J. Am. Chem. Soc.* **1986**, *108*, 2093−2094.
(25) Rutar, A. Suppression of Homonuclear J Couplings in Proton-Carbon-13 Chemical-shift Correlation Maps. *J. Magn. Reson.* **1984**, *59*, 306−310.
(26) Bax, A.; Freeman, R. Two-Dimensional NMR in Liquids. *J. Magn. Reson.* **1981**, *44*, 542−561.
(27) Wong, T. C.; Rutar, V. Homonuclear Decoupling in Heteronuclear Chemical Shift Correlation Spectroscopy. I. Study of Progesterone. *J. Am. Chem. Soc.* **1984**, *106*, 7380−7384.
(28) Bax, A. Structure Determination and Spectral Assignment by Pulsed Polarization Transfer *via* Long-Range 1H-13C Couplings. *J. Magn. Reson.* **1984**, *57*, 314−318.
(29) Gharbi-Benarous, J.; Delaforge, M.; Jankowski, C. K.; Girault, J. P. A Comparative NMR Study Between the Macrolide Antibiotic Roxithromycin and Erythromycin A with Different Biological Properties. *J. Med. Chem.* **1991**, *34*, 1117−1125.
(30) Bertho, G.; Ladam, P.; Gharbi-Benarous, J.; Delaforge, M.; Girault, J. P. Solution Conformation of Methylated Macrolide Antibiotics Roxithromycin and Erythromycin using NMR and Molecular Modelling. Ribosome-bound Conformation Determined by TRNOE and Formation of Cytochrome P450-metabolite Complex. *Int. J. Biol. Macromol.* **1998**, *22*, 103−127.
(31) Haasnoot, C. A. G.; De Leeuw, F.; Altona, C. The Relationship between Proton−Proton NMR Coupling Constants and Substituent Electronegativities. An Empirical Generalization of the Karplus Equation. *Tetrahedron.* **1980**, *36*, 2783−2792.
(32) Tvaroska, I.; Hricovini, M.; Petrakova, E. An Attempt to Derive a New Karplus-Type Equation of Viscinal Proton-Carbon Coupling Constants for C−O−C−H Segments of Bonded Atoms. *Carbohydr. Res.* **1989**, *189*, 359−362.
(33) Ladam, P.; Gharbi-Benarous, J.; Piotto, M.; Delaforge, M.; Girault, J. P. Determination of Long-Range 13C-1H Coupling Constants of Macrolide Antibiotics by 2D J-δ Selective INEPT Experiment. *Magn. Reson. Chem.* **1994**, *32*, 1−7.
(34) Testa, B. *Principles of Organic Stereochemistry*; Dekker: New York, 1979; pp 112−113.
(35) Burt, S. K.; Mackay, D.; Hagler, A. T. *Computer-Aided Drug Design*; M. D. T. J. Perun and C. L. Propst Inc.: New York and Basel, 1989.
(36) Dauber-Osguthorpe, P.; Roberts, V. A.; Osguthorpe, D. J.; Wolff, J.; Genest, M.; Hagler, A. T. Structure and Energetics of Ligand Binding to Proteins: *E. coli* Dihydrofolate Reductase-Trimethoprim, A Drug-Receptor System. *Proteins: Struct., Funct., Genet.* **1988**, *4*, 31−47.
(37) van Gunsteren, W. F.; Berendsen, H. J. C. Computer Simulation of Molecular Dynamics: Methodology, Applications, and Perspectives in Chemistry. *Angew. Chem., Int. Ed. Engl.* **1990**, *29*, 992−1023.
(38) Weiner, S. J.; Kollmann, P.; Case, D. A.; Singh, U. C.; Ghio, C.; Alagona, G.; Profeta, S.; Weiner, P. A New Force Field for Molecular Mechanical Simulation of Nucleic Acids and Proteins. *J. Am. Chem. Soc.* **1984**, *106*, 765−784.
(39) Everett, J. R.; Hatton, I. K.; Tyler, J. W. Conformational Analysis of Erythromycin a Derivatives: A Predictive Method Using NMR Chemical Shift and Coupling Constant Data. *Magn. Reson. Chem.* **1990**, *28*, 114−118.
(40) Gharbi-Benarous, J.; Ladam, P.; Delaforge, M.; Girault, J. P. Conformational Analysis of Major Metabolites of Macrolide Antibiotics Roxithromycin and Erythromycin A with Different Biological Properties by NMR Spectroscopy and Molecular Dynamics. *J. Chem. Soc., Perkin Trans. 2* **1993**, 2303−2315.
(41) Teraoka, H. Binding of Erythromycin to *Escherichia Coli* Ribosomes. *J. Antibiot.* **1971**, *24*, 302−309.
(42) Mao, J. C. H.; Putterman, M. The Intermolecular Complex of Erythromycin and Ribosome. *J. Mol. Biol.* **1969**, *44*, 347−361.
(43) Debey, P.; Hui Bon Hoa, G.; Douzou, P.; Godefroy-Colburn, T.; Graffe, M.; Grunberg-Manago, M. Ribosomal Subunit Interaction as Studied by Light Scattering. Evidence of Different Classes of Ribosome Preparations. *Biochemistry* **1975**, *14*, 1553−1559.
(44) Amand, B.; Pochon, F.; Lavalette, D. Rotationnal Diffusion of *Escherichia coli* Ribosomes. *Biochimie* **1977**, *59*, 779−784.
(45) Nirmala, N. R.; Lippens, G. M.; Hallenga, K. Theory and Experimental Results of Tranfer NOE Experiments. II. The Influence of Residual Mobility and Relaxation Centers inside the Protein on the Size of Transfer NOEs. *J. Magn. Reson.* **1992**, *100*, 25−42.
(46) Tritton, T. R. Ribosome-Chloramphenicol Interactions: A Nuclear Magnetic Resonance Study. *Arch. Biochem. Biophys.* **1979**, *197*, 10−17.
(47) Tritton, T. R. Ribosome-Tetracycline Interactions. *Biochemistry* **1977**, *16*, 4133−4138.
(48) Awan, A.; Brennan, R. J.; Regan, A. C.; Barber, J. Conformational Analysis of the Erythromycin Analogues Azithromycin and Clarithromycin in Aqueous Solution and bound to Bacterial Ribosomes. *J. Chem. Soc., Chem. Commun.* **1995**, *16*, 1653−1654.
(49) Homann, H. E.; Nierhaus, K. H. Proteins Compositions of Biosynthetic Precursors and Artifical Subparticles from Ribosomal Subunits in *Escherichia coli* K12. *Eur. J. Biochem.* **1971**, *20*, 249−257.
(50) Elliott, R. L.; Pireh, D.; Nilius, A. M.; Johnson, P. M.; Flamm, R. K.; Chu, D. T. W.; Plattner, J. J.; Or, Y. S. Novel 3-Deoxy-3-Descladinosyl-6-O-Methyl Erythromycin A Analogues. Synthesis and *In Vitro* Activity. *Bioorg. Med. Chem. Lett.* **1997**, *7*, 641−646.
(51) Dinur, U.; Hagler, A. T. Determination of Atomic Point Charges and Point Dipoles from the Cartesian Derivatives of the Molecular Dipole Moment and Second Moments, and from Energy Second Derivatives of Planar Dimers. *J. Chem. Phys.* **1989**, *91*, 2949.
(52) Dinur, U.; Hagler, A. T. The Role of Nonbond and Charge Flux in Hydrogen Bond Interactions - The Effect on Structural Changes and Spectral Shifts in Water Dimer. *J. Chem. Phys.* **1992**, *97*, 9161−9172.
(53) Harris, D. R.; McGeachin, S. G.; Mills, H. H. The Structure and Stereochemistry of Erythromycin A. *Tetrahedron Lett.* **1965**, *11*, 679−685.
(54) Jelenc, P. Rapid Purification of Highly Active Ribosomes from *Escherichia coli*. *Anal. Biochem.* **1980**, *105*, 369−374.

JM970852I